ACS APPLIED MATERIALS & INTERFACES

Research Article

www.acsami.org

High-Efficiency Phosphorescent Hybrid Organic–Inorganic Light-Emitting Diodes Using a Solution-Processed Small-Molecule Emissive Layer

Changjun Fan, Yong Lei, Zhen Liu, Ruixue Wang, Yanlian Lei, Guoqing Li, Zuhong Xiong, and Xiaohui Yang*

School of Physical Science and Technology, Southwest University, Chongqing 400715, P. R. China

Supporting Information

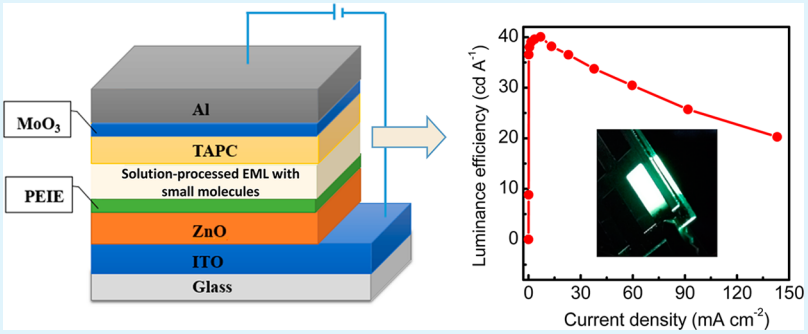

ABSTRACT: The morphology and optical and electrical properties of solution-processed and vacuum-deposited 4,4′,4″-tris(carbazol-9-yl)triphenylamine (TCTA):2,2′-(1,3-phenylene)bis[5-(4-*tert*-butylphenyl)-1,3,4-oxadiazole] (OXD-7) composite films are investigated. All of the films exhibit smooth and pinhole-free morphology, while the evaporated films possess enhanced carrier-transport properties compared to solution-processed ones. The close correlation between the carrier-transport feature and the packing density of the film is established. High-efficiency monochromatic and white phosphorescent hybrid organic–inorganic light-emitting diodes with solution-processed small-molecule emissive layers are reported: the maximum external quantum efficiencies of blue, yellow, and red devices are 18.9, 14.6, and 10.2%, respectively; white devices show a maximum luminance efficiency of 40 cd A^{-1} and a power efficiency of 20.8 lm W^{-1} at 1000 cd m^{-2}. The efficiencies of blue, red, and white devices represent significant improvement over previously reported values.

KEYWORDS: *hybrid organic–inorganic light-emitting diodes, solution-processed small-molecule films, vacuum-deposited films, carrier-transport property, packing density of the film*

1. INTRODUCTION

Hybrid organic–inorganic light-emitting diodes (HyLEDs) using air-stable metal oxide carrier-injection layers overcome several issues that may adversely affect the efficiency and stability of conventional devices such as the sensitivity of a low-work-function metal cathode- and electron-injection layer toward oxygen and moisture in the ambient and the interactions between the conducting polymer hole-injection layer and indium–tin oxide (ITO), providing a novel approach for the development of new display and solid-state lighting devices.[1−8] Metal oxides are particularly suitable to work as carrier-injection layers in HyLEDs because they possess many appealing properties, for instance, exceptional stability, ease of synthesis, visible-light transparency, high carrier mobility, and controllable surface morphology on a nanometer length scale. In 2006, Morii et al. reported the first HyLED with the structure of ITO/TiO_2/poly(9-dioctylfluorene-*alt*-benzothiadiazole) (F8BT)/MoO_3/Au, having a luminance efficiency (LE) of ca. 0.1−0.3 cd A^{-1}.[1] After intensive studies over the past decade, the LE of HyLEDs based on F8BT has been increased to 61.6 cd A^{-1}.[9] However, compared to conventional devices, the efficiency and operating stability of HyLEDs warrant further improvement.

In our opinion, there are several problems to be solved in the area of HyLEDs, which are listed as the following: (1) Conjugated polymers such as F8BT[6−11] and phenyl-substituted poly(phenylvinylene) (SY-PPV)[5,12,13] have been mainly used as the emissive layer (EML) in HyLEDs. As a result, the device efficiency is restricted by the singlet-to-triplet exciton formation ratio. Meanwhile, the low-energy nonemissive triplet excited states of conjugated polymers significantly quench the luminescence of phosphorescent emitters, which makes such polymers unsuitable to work as the host materials for phosphorescent devices. (2) Widely studied F8BT and SY-

Received: June 29, 2015
Accepted: September 3, 2015
Published: September 3, 2015

DOI: 10.1021/acsami.5b05815
ACS Appl. Mater. Interfaces 2015, 7, 20769−20778

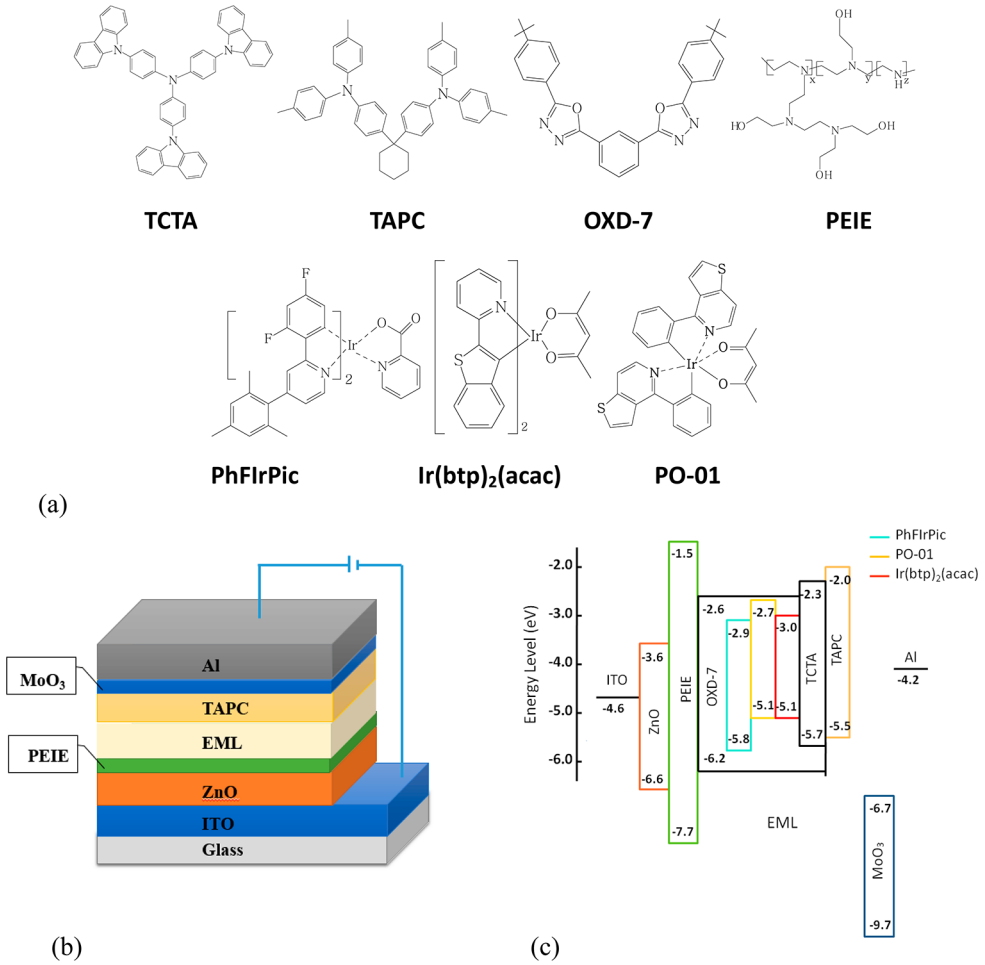

Figure 1. Chemical structures of the materials (a) and schematic configuration (b) and energy-level diagram (c) of HyLEDs.

PPV devices are all yellowish-green-emitting,[5−13] while fewer studies have focused on blue and red HyLEDs, which are, on the other hand, indispensable for the future application of HyLEDs on display devices. To date, the highest external quantum efficiencies (EQEs) of blue[14] and red[15] HyLEDs are only ca. 3%, and it is urgent to enhance the efficiency of such devices. (3) There have been few studies of white HyLEDs, probably because of the unsatisfactory performances of blue HyLEDs. Bolink et al. reported white HyLEDs with a maximum LE of 2.7 cd A^{-1} and Commission Internationale de L'Eclairage (CIE) coordinates of (0.37, 0.35), which were based on blue-emitting polymer poly(9,9-dioctylfluorenyl-2,7-diyl) (PFO) and phosphorescent orange emitter iridium(III) bis(2-methyldibenzo[*f*,*h*]quinoxaline(acetylacetonate) [Ir-$(MDQ)_2$(acac)].[16] We note that many small-molecule materials possess high triplet energy (E_T), allowing the effective confinement of triplet excited states onto phosphorescent emitters and working as ideal host materials for phosphorescent devices. High-performance conventional devices based on solution-processed small-molecule EMLs have been reported.[17] However, it is difficult to prepare high-quality small-molecule layers via a solution-processing method on widely adopted crystalline and highly polar alkali-metal or alkaline-earth-metal compounds based on electron-injection layers.[4,7,8,11,18,19] Crystallization of small-molecule components when coated on top of a Cs_2CO_3 layer has been reported by Bolink et al.[20] As such, HyLEDs using a solution-processed small-molecule EML have seldom been reported although such devices are expected to have high potential in the attainment of high-efficiency and wide-range emission wavelength tuning and can address most of the problems aforementioned. One of the crucial prerequisites for the construction of such HyLEDs is to seek novel electron-injection layers, which possess excellent electron-injection and hole/exciton-blocking capability and, more importantly, have benign compatibility with the overlying small-molecule EML.[21,22] In this regard, we note that polyethylenimine ethoxylated (PEIE) can significantly enhance electron-injection from metal oxides to various organic functional layers[23,24] and would not significantly disturb the morphology of the adjacent small-molecule EML because the surface energy of PEIE is closer to that of EML compared to that of alkali-metal or alkaline-earth-metal compounds. Recently, we have reported green HyLEDs using a solution-processed small-molecule EML with a maximum LE of 87.6 cd A^{-1}.[25]

In this article, we investigate the effects of processing solvents and thermal treatment on the morphology and optical and electrical characteristics of small-molecule composite layers. A direct comparison with the properties of the evaporated counterpart is also made. Further, we report highly efficient monochromatic and white HyLEDs based on solution-processed small-molecule EMLs: the maximum EQEs of blue, yellow, and red devices are 18.9, 14.6, and 10.2%, respectively;

DOI: 10.1021/acsami.5b05815
ACS Appl. Mater. Interfaces 2015, 7, 20769−20778

the maximum LE of white HyLEDs is 40 cd A^{-1}, and the power efficiency (PE) at 1000 cd m^{-2} is 20.8 lm W^{-1}.

2. EXPERIMENTAL SECTION

Materials. PEIE-modified ZnO is used as the electron-injection layer for an ITO cathode, and MoO_3 and 1,1-bis[(di-4-tolylamino)-phenyl]cyclohexane (TAPC) are used as hole-injection and hole-transport layers, respectively. The hole-transporting material 4,4′,4″-tris(carbazol-9-yl)triphenylamine (TCTA) and the electron-transporting material 2,2′-(1,3-phenylene)bis[5-(4-*tert*-butylphenyl)-1,3,4-oxadiazole] (OXD-7) are employed as the cohosts in an EML. Bis[2-(4,6-difluorophenyl)-4-(2,4,6-trimethylphenyl)pyridinato-C^2,N]-(picolinato)iridium(III) (PhFIrPic), iridium(III) bis(4-phenylthieno-[3,2-*c*]pyridinato-N,C^2)acetylacetonate (PO-01), and bis(2-benzo[*b*]-thiophen-2-yl-pyridine)(acetylacetonate)iridium(III) [$Ir(btp)_2(acac)$] are used as blue, orange, and red phosphorescent emitters, respectively. PhFIrPic possesses optoelectronic properties similar to those of the parent bis[(4,6-difluorophenyl)pyridinato-N,C^2]-(picolinate)iridium(III) (FIrPic) and exhibits good solubility in organic solvents like chlorobenzene (CB). Chemical structures of the materials are shown in Figure 1a.

Device Fabrication. The schematic configuration and energy-level diagram of HyLEDs are shown in Figure 1b,c, respectively. The highest occupied molecular orbital (HOMO) and lowest unoccupied molecular orbital (LUMO) levels of organic materials, the conduction and valence band onsets of metal oxides, and the work function of the electrodes are cited from the literature.[25−28] ZnO layers were prepared by spin-coating a 2-methoxyethanol solution of zinc acetate dihydrate on top of precleaned ITO substrates and annealing the resultant films at 200 °C for 1 h in air.[29] ZnO layers were rinsed with 2-methoxyethanol in order to remove unreacted zinc acetate. A poly(3,4-ethylenedioxythiophene)/poly(styrenesulfonate) (PEDOT:PSS) layer was prepared by spin-coating its aqueous dispersion onto ITO substrates, which was then heated at 170 °C for 10 min under an ambient atmosphere. A PEIE layer was deposited from its 2-methoxyethanol solution onto a ZnO layer. The substrates were then transferred into the glovebox, where a TCTA:OXD-7:phosphorescent emitter layer was applied on top of the PEIE layer from the CB solution. The thicknesses of the ZnO, PEDOT:PSS, and PEIE layers were measured by a Dektak surface stylus profiler as 30, 50, and 10 nm, respectively. The samples were loaded into a high-vacuum chamber that resided inside the glovebox without exposure to air, in which 60 nm TAPC, 10 nm MoO_3, and 100 nm aluminum as the hole-transport layer, hole-injection layer, and anode, respectively, were sequentially evaporated under a pressure of less than 1×10^{-4} Pa. The thicknesses of the evaporated layers were determined by a quartz crystal oscillator. For electron-only devices, a top contact with a structure of OXD-7 (40 nm)/CsF (1 nm)/Al (100 nm) was made. For hole-only devices, the ZnO/PEIE bilayer in light-emitting devices was replaced by a PEDOT:PSS layer. Current density−luminance−voltage (I−L−V) characteristics were measured by a Keithley 2400 electrometer and a Konica−Minolta Chroma Meter CS-100A, which were controlled by a homemade *Labview* program. An Ocean Optics USB4000 UV−vis diffractometer was used to record the electroluminescent (EL) spectra. The surface morphology of organic layers was measured by atomic force microscopy (AFM; Hitachi microscope). Ellipometry measurements were carried out with a W-VASE with an Auto Retarder TM.

3. RESULTS AND DISCUSSION

TCTA and OXD-7 have been used as hole- and electron-transport materials for a long time because they possess relatively high hole and electron mobility of 10^{-4} and 10^{-5} cm^2 V^{-1} s^{-1}.[30,31] To investigate the effect of processing solvents and heat treatment on the properties of small-molecule films, we prepare TCTA:OXD-7 (1:1 by weight) layers from a CB and tetrahydrofuran (THF) solution on top of bare or PEIE/ZnO bilayer precoated glass substrates and anneal some layers

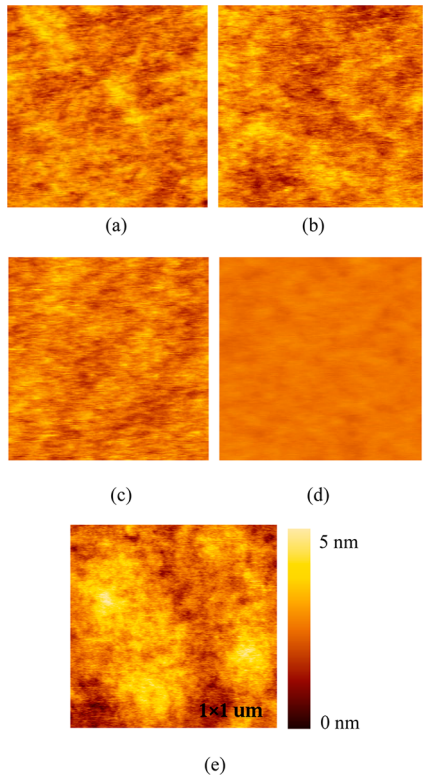

Figure 2. AFM images of solution-processed TCTA:OXD-7 films deposited from CB (a), from THF (b), from THF and subsequently annealed (c), and from a vacuum-deposited film (d) on glass substrates as well as that of the sample prepared from CB on top of PEIE/ZnO (e).

processed from THF at 80 °C for 10 min. Vacuum-deposited TCTA:OXD-7 layers are also made for comparison. The morphology and optical and electrical properties of the TCTA:OXD-7 films have been studied. Figure 2 shows the AFM images of the samples. The root-mean-square (rms) roughness values of the layers on glass substrates processed from CB and THF are both 0.29 nm, which is similar to those of annealed (0.26 nm) and evaporated (0.23 nm) layers, as shown in Figure 2a−d. The rms roughness value of the samples on top of the PEIE/ZnO layer is ca. 1 nm (Figure 2e), which is larger than those of the samples on glass substrates. We reported that PEIE formed island-like structures on ITO, exhibiting a rms roughness of 3.4 nm.[32] The enhanced rms roughness of the TCTA:OXD-7 layer on top of PEIE/ZnO may be partially associated with the roughness of the underlying PEIE layer. All of the films show a pinhole-free and smooth surface. Lee et al. reported the effect of processing solvents on the morphology of 2-(*tert*-butyl)-9,10-bis(2′-naphthyl)anthracene (TBADN)/4,4′-bis[2-[4-(*N*,*N*-diphenylamino)phenyl]vinyl] (DPAVBi) films. The rms roughness values of films obtained from a CB and toluene solution were 0.52 and 0.66 nm, respectively. A kind of aggregation is present in the film prepared from a toluene solution.[33] In contrast, few aggregates can be observed in the TCTA:OXD-7 films, which can be attributed to reduced intermolecular interactions because of the three-dimensional molecular structure of TCTA[34] and spatial hindrance from the *tert*-butyl group in the OXD-7 structure.[17]

The single-carrier devices have been prepared to investigate the electrical properties of the TCTA:OXD-7 films. Figure 3a

DOI: 10.1021/acsami.5b05815
ACS Appl. Mater. Interfaces 2015, 7, 20769−20778

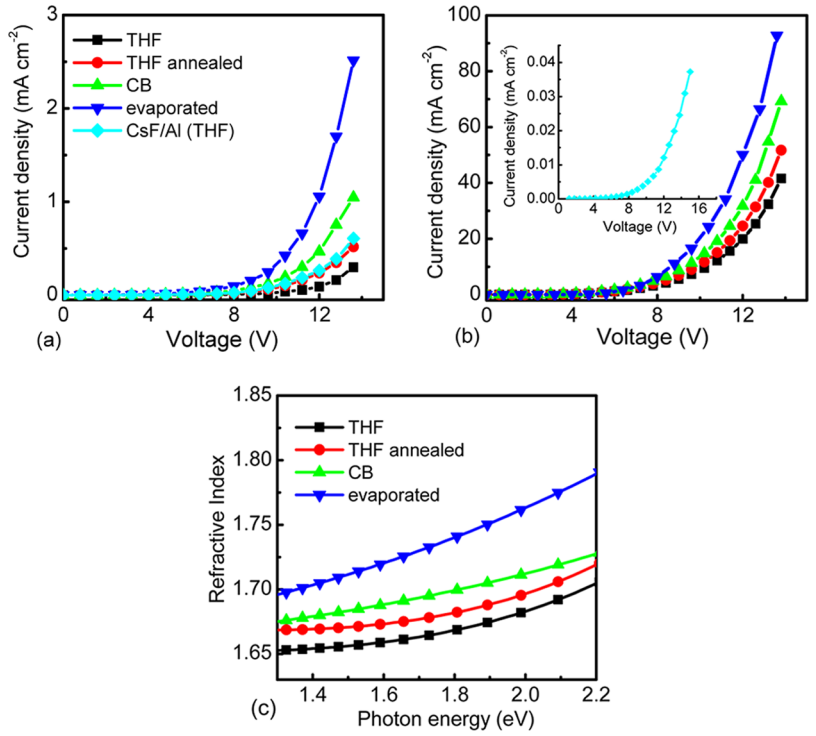

Figure 3. Current density−voltage characteristics of electron-only devices (a), current density−voltage characteristics of the hole-only devices with various TCTA:OXD-7 layers using either MoO_3/Al (b) or PEDOT:PSS hole-injection contact (inset of part b), and the refractive indices of TCTA:OXD-7 samples (c).

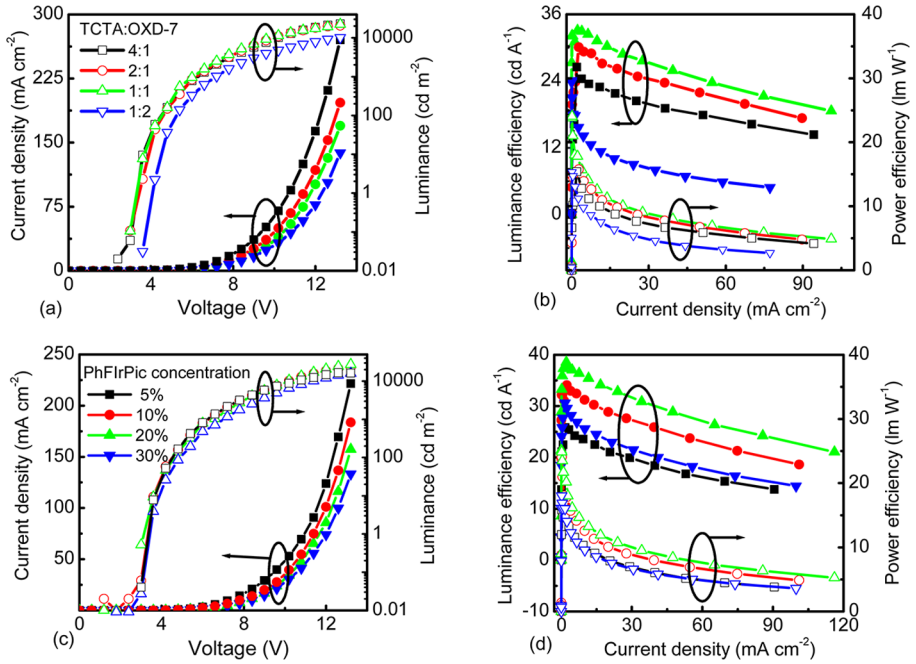

Figure 4. *I*−*L*−*V* (a) and *I*−LE−PE curves (b) of the blue HyLEDs employing different TCTA:OXD-7 ratios. *I*−*L*−*V* plots (c) and *I*−LE−PE properties (d) of the blue HyLEDs using different PhFIrPic concentrations.

shows the current density−voltage characteristics of the electron-only devices with the structure of ITO/ZnO/PEIE/TCTA:OXD-7 (1:1, 70 nm)/OXD-7 (40 nm)/CsF/Al. For the device with a TCTA:OXD-7 layer processed from THF and subsequently annealed, the current densities for injection of electrons from both ITO/ZnO/PEIE and CsF/Al are almost identical, indicating that the ZnO/PEIE bilayer possesses electron-injection capability similar to that of a commonly practiced efficient CsF electron-injection layer. The work function of ZnO is about 4 eV, lower than that of ITO (4.3−4.6 eV). Thus, ZnO works as an electron injector for some polymers with a deep-lying LUMO level such as F8BT.[2] The addition of a PEIE layer on top of ZnO largely reduces the work function to ca. 3.3 eV because of the formation of

DOI: 10.1021/acsami.5b05815
ACS Appl. Mater. Interfaces 2015, 7, 20769−20778

Table 1. Comparison of the Properties of HyLEDs

device	V_{on}	LE_{max} (cd A^{-1})	PE_{max} (lm W^{-1})	EQE_{max} (%)	CIE
blue	3.0	38.5	25.1	18.9	(0.16, 0.36)
blue[a]	≈7.5	6.0	≈1.8	3.1	(0.19, 0.24)[14]
yellow	2.4	46.1	33.2	14.6	(0.49, 0.50)
yellow[a]	2.6	61.6	19.4	17.8	NA[9]
red	3.0	9.7	5.1	10.2	(0.66, 0.32)
red[a]	≈1.8	2.0	≈1.4	3.2	NA[15]
white (two-element)	2.4	40.0	30.0	15.0	(0.33, 0.44)
white (three-element)	3.0	27.6	16.4	10.9	(0.38, 0.47)
white[a]	≈2.0	2.7	≈1.5	N.A	(0.37, 0.35)[16]

[a]Values for monochromatic and white HyLEDs in the literature.

interfacial dipoles, thus facilitating electron injection.[23] At a given voltage, the current density of the device with an evaporated layer ($I_{electron,EV}$) is larger than that of the device with a solution-processed layer despite the fact that all of the TCTA:OXD-7 films show similar morphology. Among the devices with a solution-processed TCTA:OXD-7 layer, the current density of the device processed from CB ($I_{electron,CB}$) exceeds that of the device processed from THF ($I_{electron,THF}$). It is also worth noting that heat treatment of films leads to a slight increase in the current density ($I_{electron,ANN}$). It is important that $I_{electron,CB}$ is only 1.6 times lower than $I_{electron,EV}$. Thus, our results indicate that, apart from smooth surface morphology, solution-processed TCTA:OXD-7 layers on top of PEIE/ZnO possess reasonable carrier-transport properties, which enable them to work properly in light-emitting devices. Figure 3b shows the current density–voltage characteristics of the hole-only devices with the structure of ITO/PEDOT:PSS/TCTA:OXD-7 (70 nm)/TAPC (110 nm)/MoO_3/Al. The current density for injection of holes from MoO_3/Al is 3 orders of magnitude higher than that from ITO/PEDOT:PSS (inset of Figure 3b). There is a large energy barrier for hole injection from PEDOT:PSS with a work function of 5.1 eV[35] into the HOMO level of TCTA (−5.7 eV), while MoO_3 with a work function of 6.6 eV[36] delivers almost barrier-free hole injection (Figure 1c). The electron current density is more than 1 order of magnitude lower than the hole current density upon injection from MoO_3/Al, which can be explained by the fact that the hole mobility of TCTA is ca. 10 times larger than the electron mobility of OXD-7. Interestingly, the effects of the film-forming process on the hole and electron current density are similar: the hole current density at certain voltages increases in the sequence of $I_{hole,THF} < I_{hole,ANN} < I_{hole,CB} < I_{hole,EV}$.

We further measure the refractive indices of the films using spectroscopic ellipometry. Figure 3c shows the refractive indices of the samples. The refractive index of the vacuum-deposited film is larger than those of the solution-processed films, which can be attributed to the lower packing density and the existence of free volume in the solution-processed samples. Among the samples with a solution-processed layer, the sample obtained from CB shows a larger refractive index than the sample prepared from THF. Meanwhile, heat treatment increases the refractive index of the film. Thus, the close correlation between the refractive index and carrier-transport property of the TCTA:OXD-7 layer is established. Similar observation of a lower operating voltage for devices employing the vacuum-deposited *N*,*N*-bis(1-naphthalenyl)-*N*,*N*-bis-(phenylbenzidine) (NPB)/1,3,5-tris(*N*-phenylbenzimidazol-2-yl)benzene (TPBI) films compared to those with solution-processed films has been attributed to the higher packing density and the resultant larger carrier mobility in the vacuum-deposited films by Kim et al.[37] On the other hand, Lee et al. reported that a higher current density was measured in devices

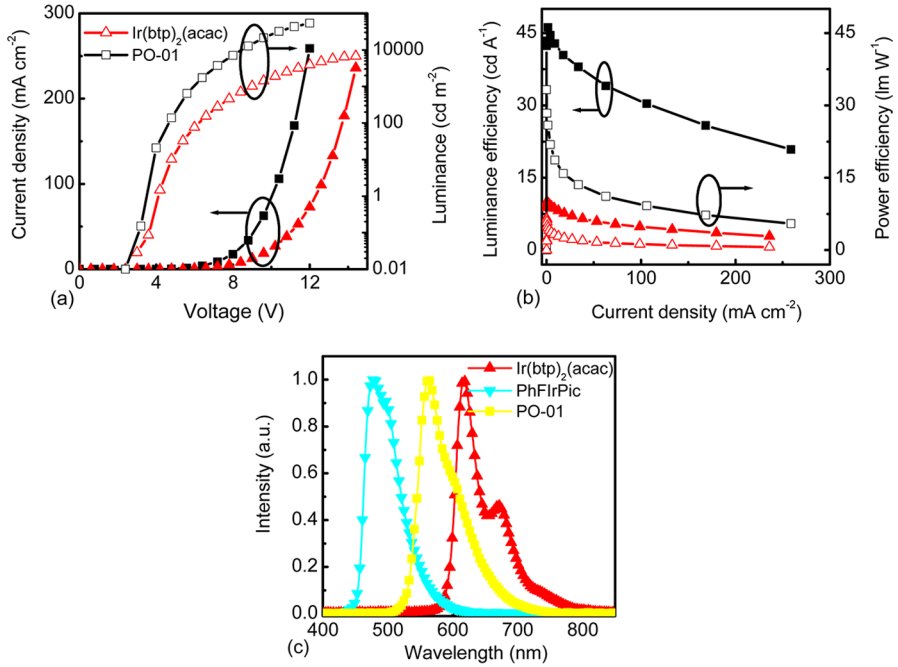

Figure 5. Characteristics of the yellow and red HyLEDs: *I*–*L*–*V* plots (a), *I*–LE–PE characteristics (b), and EL spectra of the blue, yellow, and red devices (c).

DOI: 10.1021/acsami.5b05815
ACS Appl. Mater. Interfaces 2015, 7, 20769–20778

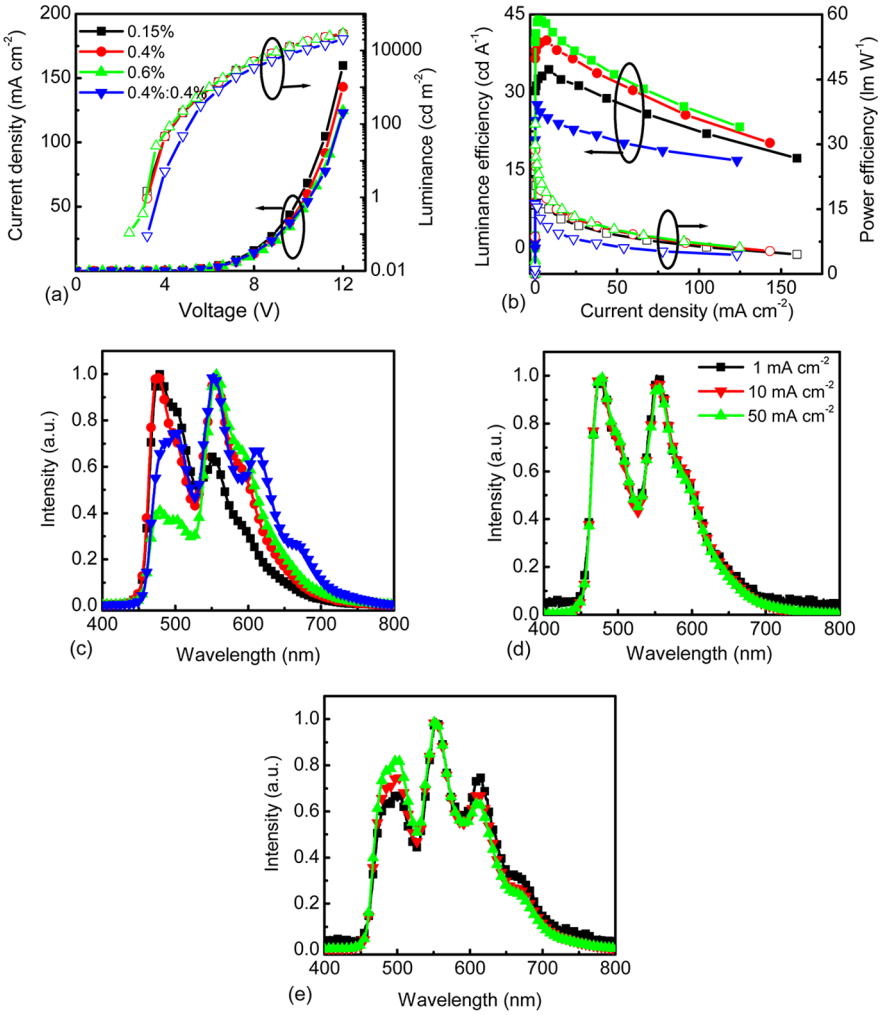

Figure 6. Characteristics of HyLEDs with two or three phosphorescent emitters: $I-L-V$ plots (a); I−LE−PE properties (b); EL spectra of the devices at 10 mA cm^{-2} (c); EL spectra of the devices with EML containing 20% PhFIrPic and 0.4% PO-01 under different current densities (d); EL spectra of the devices with EML containing 20% PhFIrPic, 0.4% PO-01, and 0.4% Ir(btp)$_2$(acac) under different current densities (e).

using solution-processed TBADN/DPAVBi layers with lower packing density with respect to those having the vacuum-deposited layer, which was associated with facilitation of carrier transport by aggregates.[33] The formation of *N*,*N*′-bis(3-methylphenyl)-*N*,*N*′-diphenyl-(1,1′-biphenyl)-4,4-diamine (TPD) aggregates is proposed to lead to more compact intermolecular stacking and higher hole mobility for solution-processed films compared to the vacuum-deposited counterpart.[38] Although how the film-forming process affects the carrier-transport property may be material-dependent, our results agree with those reported by Kim et al.[37] Because the influences of processing solvent and heat treatment on the hole- and electron-transport properties of the TCTA:OXD-7 film are similar, we speculate that varied carrier-transport properties can mainly be attributed to different packing densities but not to alteration of the TCTA and OXD-7 distribution inside the film.

Recently, TCTA and OXD-7 have been used as the host materials for FIrPic because the E_T values of TCTA (2.78 eV) and OXD-7 (2.7 eV) are higher than that of FIrPic (2.65 eV).[30,39−41] In addition, utilization of TCTA:OXD-7 cohosts allows for the fine adjustment of the carrier-transport balance in an EML. We fabricate a serial blue HyLEDs with the structure of ITO/ZnO/PEIE/TCTA:OXD-7:10% PhFIrPic (70 nm)/TAPC (60 nm)/MoO_3/Al to investigate the effects of different TCTA:OXD-7 ratios on the device performance. Figure 4 shows the $I-L-V$ and current density−luminance efficiency−power efficiency (I−LE−PE) characteristics of the blue HyLEDs with different ratios of TCTA and OXD-7. As shown in Figure 4a, the current density at a certain voltage increases with increasing TCTA concentration, which can be attributed to different hole and electron mobilities for TCTA and OXD-7. All of the devices show similar light-emission onset voltage (V_{on}) of ca. 3.0 V and a maximum luminance of ca. 20000 cd m^{-2}. Figure 4b compares the I−LE−PE characteristics of the devices. The maximum LE of the device increases with a decrease in the TCTA:OXD-7 ratio from 4:1 to 1:1. Notably, the maximum LE and PE of 34.0 cd A^{-1} and 24.1 lm W^{-1} are obtained in the device with a TCTA:OXD-7 ratio of 1:1. Detailed device properties are summarized in Table S1 in the Supporting Information (SI). Because carrier transport in an EML is dominated by holes, an increase of the OXD-7 content helps to balance carrier transport, thereby enhancing the device efficiency. However, the maximum LE decreases to 25.2 cd A^{-1} with a further decrease of the TCTA:OXD-7 ratio to 1:2, and at the same time, the LE−I plot shows a sharp LE roll-off at high current densities. We find that layers with this composition on either glass substrates or ZnO/PEIE layers

DOI: 10.1021/acsami.5b05815
ACS Appl. Mater. Interfaces 2015, 7, 20769−20778

appear milky and birefringent, implying that crystallization may occur in the film.

As the next step, we study the influence of the PhFIrPic concentration on the properties of blue HyLEDs. The characteristics of the devices with PhFIrPic concentrations of 5, 10, 20, and 30% are shown in Figure 4c,d. The operating voltage at a given current density increases with increasing PhFIrPic concentration. As indicated by the energy-level diagram of the device (Figure 1c), the LUMO level of PhFIrPic is located at ca. −3.2 eV, which is lower than that of OXD-7 (ca. −2.7 eV). Therefore, PhFIrPic works as an electron trap in the EML, which may account for decreased current density with increasing PhFIrPic concentration. Lee et al.[42] reported that higher current density and LE were measured in stepwise doped devices having larger FIrPic concentration at the EML/electron-transport layer interface, which was attributed to direct injection of electrons into FIrPic and electron hopping among FIrPic sites. To examine this point, we prepare the single-electron devices with various PhFIrPic concentrations and find that the current density decreases with increasing PhFIrPic concentration (Figure S1 in the SI). It appears that electron hopping among PhFIrPic sites plays a minor role in the present case. LE of the device increases with an increase in the PhFIrPic concentration from 5 to 20%. The maximum LE and PE of 38.5 cd A^{-1} and 25.1 lm W^{-1} are measured for the 20% PhFIrPic device (Table S2 in the SI). At 1000 cd m^{-2}, LE and PE of the device are 38 cd A^{-1} and 18.4 lm W^{-1}. Further, LE of the device is almost independent of the EML thickness ranging from 70 to 110 nm (Figure S2 in the SI). Baldo et al. introduced the characteristic current density at which the device efficiency falls to half of its maximum.[43] The characteristic current density value of the 20% PhFIrPic device is as large as 136.1 mA cm^{-2}, which is among the best values for solution-processed FIrPic devices (Table S3 in the SI). Rather small efficiency roll-off at high current densities can be attributed to alleviated triplet−triplet and triplet−polaron interactions in a broad carrier recombination zone due to the use of hole-transporting TCTA and electron-transporting OXD-7 as the cohosts.[44,45] The 30% PhFIrPic device shows a maximum LE of ca. 31 cd A^{-1} and at the same time a reduced characteristic current density of 97.3 mA cm^{-2}. Enhanced triplet−triplet and triplet−polaron interactions may account for reduction of the device efficiency in this case. The maximum EQE of the 20% PhFIrPic device (18.9%) represents significant improvement over the previously reported value,[14] which can be mainly attributed to the effective utilization of triplet excited states for light emission enabled by the introduction of phosphorescent emitters into small-molecule cohosts. A detailed comparison of the properties of HyLEDs is presented in Table 1. Furthermore, it should be noted that the EQE of the blue HyLEDs rivals those of the state-of-the-art solution-processed blue-emitting conventional devices.[17]

Encouraged by the impressive results of the blue HyLEDs based on a solution-processed small-molecule EML, we proceed to study yellow and red HyLEDs by using PO-01 and $Ir(btp)_2(acac)$ as the yellow and red phosphors. The optimal PO-01 concentration is determined to be 10% (Figure S3 in the SI). Figure 5 shows the properties of the yellow HyLEDs with the structure of ITO/ZnO/PEIE/TCTA(1):OXD-7(1):10% PO-01 (50 nm)/TAPC (60 nm)/MoO_3/Al. V_{on} of the yellow HyLEDs is 2.4 V, and the maximum luminance reaches 63000 cd m^{-2}. The maximum LE and PE are 46.1 cd A^{-1} and 33.2 lm W^{-1}, which slightly decrease to 45.6 cd A^{-1} and 24.6 lm W^{-1} at 1000 cd m^{-2}. Red HyLEDs with 10% $Ir(btp)_2(acac)$ show the best performance (Figure S4 in the SI). The properties of the red HyLEDs with the structure of ITO/ZnO/PEIE/TCTA(1):OXD-7(1):10% $Ir(btp)_2(acac)$ (70 nm)/TAPC (60 nm)/MoO_3/Al are also included in Figure 5. The maximum LE and PE for the red HyLEDs are 10.0 cd A^{-1} and 6.6 lm W^{-1}, and the corresponding values at 1000 cd m^{-2} are 8.1 cd A^{-1} and 2.9 lm W^{-1}. As presented in Table 1, EQEs of the present devices are among the highest values for yellow and red HyLEDs, which are comparable to those of solution-processed conventional devices based on PO-01[46] and $Ir(btp)_2(acac)$.[47] The selection of phosphors with enhanced luminescence quantum yields would increase the LE values of the devices.[48] The characteristic current density values of the yellow and red HyLEDs exceed 100 mA cm^{-2}, which is similar to that of the blue HyLEDs, highlighting the fact that utilization of small-molecule cohosts is effective in maintaining the device efficiency at high current densities. The EL spectra of the blue, yellow, and red HyLEDs (Figure 5c) peak at 475, 563, and 617 nm, which can be assigned to the respective emission from PhFIrPic, PO-01, and $Ir(btp)_2(acac)$. The devices exhibit CIE coordinates of (0.16, 0.36), (0.49, 0.50), and (0.66, 0.32), respectively, which almost traverse the whole visible-light region.

On the basis of the above results of monochromatic HyLEDs, we go further to explore white HyLEDs by using PhFIrPic and PO-01 as blue and yellow phosphors. Figure 6a shows the $I-L-V$ characteristics of HyLEDs with the structure of ITO/ZnO/PEIE/TCTA(1):OXD-7(1):20% PhFIrPic:x% PO-01 (70 nm)/TAPC (60 nm)/MoO_3/Al, in which x is 0.15, 0.4, or 0.6. As shown in Figure 6a, variation of the PO-01 concentration only slightly affects the current density−voltage characteristics. The maximum LE and PE of 44.0 cd A^{-1} and 34.6 lm W^{-1} (Figure 6b) are obtained in the 0.6% PO-01 device. The intensive peaks at 475 and 553 nm in the EL spectra come from PhFIrPic and PO-01, as shown in Figure 6c. The relative PhFIrPic emission intensity significantly decreases with increasing PO-01 concentration, and PO-01 emission is dominant in the EL spectrum of the 0.6% PO-01 device. The 0.15, 0.4, and 0.6% PO-01 devices have CIE coordinates of (0.28, 0.43), (0.33, 0.44), and (0.40, 0.48) at 10 mA cm^{-2}, respectively. Among the devices, CIE coordinates of the 0.4% PO-01 device are the closest to the white point (0.33, 0.33). The maximum EQE and PE of the 0.4% PO-01 device are 15.0% and 30.0 lm W^{-1}, and the corresponding values are 14.7% and 20.6 lm W^{-1} at 1000 cd m^{-2}. Holes and electrons injected from MoO_3/Al and PEIE/ZnO/ITO contacts recombine in the EML, forming excitons of host materials. Subsequently, energy transfer from the host materials to phosphors and from PhFirPic to PO-01 populates excited states of PhFirPic and PO-01. As shown in the energy-level diagram of the device (Figure 1c), PhFIrPic works as an electron trap and PO-01 mainly acts as a hole trap in an EML, leading to the direct formation of PhFirPic and PO-01 excited states. Blue and yellow emission intensities in EL spectra can be adjusted by varying the PhFIrPic and PO-01 concentrations in the EML. The relative PhFIrPic emission intensity slightly increases with an increase in the current density from 1 to 50 mA cm^{-2} (Figure 6d), leading to very subtle changes of the CIE coordinates from (0.32, 0.43) to (0.32, 0.44). Two-element white devices typically show a rather moderate color rendering index (CRI) value because of the fact that EL spectra fail to

DOI: 10.1021/acsami.5b05815
ACS Appl. Mater. Interfaces 2015, 7, 20769−20778

completely cover the whole visible-light region. To improve the CRI value of white HyLEDs, red phosphor $Ir(btp)_2(acac)$ is introduced into the EML. The $I-V$ characteristics of the three-element devices with the structure of ITO/ZnO/PEIE/TCTA(1):OXD-7(1):20% PhFIrPic:0.4% PO-01:0.4% $Ir(btp)_2(acac)$ (70 nm)/TAPC (60 nm)/MoO_3/Al are similar to those of the two-element devices (Figure 6a). The device exhibits the maximum EQE and PE of 10.9% and 16.4 lm W^{-1}. The addition of $Ir(btp)_2(acac)$ decreases the device efficiency because of the relatively low EQE of the $Ir(btp)_2(acac)$ device, as mentioned above. The EL spectrum of the three-element devices (Figure 6c) contains emission peaks at 475, 553, and 610 nm coming from PhFIrPic, PO-01, and $Ir(btp)_2(acac)$, respectively. Also, the CIE coordinates and CRI value have been measured to be (0.38, 0.47) and 71. There is a noticeable increase of the relative PhFIrPic emission intensity and concomitant reduction of the relative $Ir(btp)_2(acac)$ emission intensity with an increase in the current density from 1 to 50 mA cm^{-2} (Figure 6e), leading to variation of the CIE coordinates from (0.39, 0.46) to (0.36, 0.47).

The PO-01 device driven at an initial luminance of 600 cd m^{-2} shows ca. 50% decrease in luminance during a period of 0.3−0.5 h (Figure S5 in the SI). The operating lifetime of inverted devices using a PEI/ZnO electron-injection layer and a SY-PPV EML at 500 cd m^{-2} is reported to be ca. 20 h,[5] while similar devices using ethanolamine-treated ZnO as the electron-injection layer show good stability,[49] indicating that degradation of the devices may be partially related to PEI or the chemically related PEIE layer. In addition, solution-processed devices show inferior stability compared to the vacuum-deposited analogue, probably because of the low packing density of the solution-processed films and residual solvent inside the films.[33] Further efforts are underway to improve the operating stability of the devices.

4. CONCLUSION

Our results indicate that solution-processed TCTA:OXD-7 layers possess smooth and pinhole-free morphology as well as reasonable carrier-transport properties, which render them to work properly in HyLEDs. Selection of the proper processing solvent and heat treatment can effectively improve the carrier-transport property of a solution-processed TCTA:OXD-7 layer. The close correlation between the packing density and carrier-transport property for the TCTA:OXD-7 layer is established. Blue, yellow, and red HyLEDs with solution-processed TCTA:OXD-7:phosphor EMLs show maximum EQEs of 18.9, 14.6, and 10.2%, respectively. In addition, white HyLEDs based on the same methodology show a high EQE of 15.0% and current-density-insensitive CIE coordinates of (0.33, 0.44). The efficiencies of blue, red, and white devices represent a significant improvement over previously reported values. In addition, the characteristic current density values of the devices exceed 100 mA cm^{-2}, which are among the best reported values for solution-processed devices. Thus, utilization of solution-processed small-molecule EMLs serves as a general approach to achieving highly efficient monochromatic and white HyLEDs.

■ ASSOCIATED CONTENT

Supporting Information

The Supporting Information is available free of charge on the ACS Publications website at DOI: 10.1021/acsami.5b05815.

Influence of the PhFIrPic concentration on the electron current, characterization of PhFIrPic devices with various EML thicknesses, properties of the yellow and red HyLEDs with different phosphor concentrations, summary of the properties of the blue HyLEDs using different EML compositions, and comparison of the characteristic current densities of the solution-processed devices using different small-molecule host materials and stability measurements (PDF)

■ AUTHOR INFORMATION

Corresponding Author

*E-mail: xhyang@swu.edu.cn.

Notes

The authors declare no competing financial interest.

■ ACKNOWLEDGMENTS

Financial support by the National Natural Science Foundation of China (Grants 61177030, 11474232, 11374242, and 11204247), the Chinese Ministry of Education under the program for New Century Excellent Talents in Universities (Grant NCET-11-0705), and the start-up Grant SWU111057 from Southwest University is acknowledged.

■ REFERENCES

(1) Morii, K.; Ishida, M.; Takashima, T.; Shimoda, T.; Wang, Q.; Nazeeruddin, M. K.; Grätzel, M. Encapsulation-Free Hybrid Organic-Inorganic Light-Emitting Diodes. *Appl. Phys. Lett.* **2006**, *89*, 183510.

(2) Sessolo, M.; Bolink, H. J. Hybrid Organic-Inorganic Light-Emitting Diodes. *Adv. Mater.* **2011**, *23*, 1829−1845.

(3) Kabra, D.; Song, M. H.; Wenger, B.; Friend, R. H.; Snaith, H. J. High Efficiency Composite Metal Oxide-Polymer Electroluminescent Devices: A Morphological and Material Based Investigation. *Adv. Mater.* **2008**, *20*, 3447−3452.

(4) Morii, K.; Kawase, T.; Inoue, S. High Efficiency and Stability in Air of the Encapsulation-Free Hybrid Organic-Inorganic Light-Emitting Diode. *Appl. Phys. Lett.* **2008**, *92*, 213304.

(5) Kim, Y. H.; Han, T. H.; Cho, H.; Min, S. Y.; Lee, C. L.; Lee, T. W. Polyethylene Imine as an Ideal Interlayer for Highly Efficient Inverted Polymer Light-Emitting Diodes. *Adv. Funct. Mater.* **2014**, *24*, 3808−3814.

(6) Bolink, H. J.; Coronado, E.; Repetto, D.; Sessolo, M.; Barea, E. M.; Bisquert, J.; Garcia-Belmonte, G.; Prochazka, J.; Kavan, L. Inverted Solution Processable OLEDs Using a Metal Oxide as an Electron Injection Contact. *Adv. Funct. Mater.* **2008**, *18*, 145−150.

(7) Huang, C. Y.; Yang, C. C.; Yu, H. C.; Chen, Y. C. Impact of Preparation Condition of ZnO Electron Transport Layer on Performance of Hybrid Organic-Inorganic Light-Emitting Diodes. *J. Appl. Phys.* **2014**, *115*, 083109.

(8) Lu, L. P.; Kabra, D.; Friend, R. H. Barium Hydroxide as an Interlayer Between Zinc Oxide and a Luminescent Conjugated Polymer for Light-Emitting Diodes. *Adv. Funct. Mater.* **2012**, *22*, 4165−4171.

(9) Lee, B. R.; Jung, E. D.; Park, J. S.; Nam, Y. S.; Min, S. H.; Kim, B. S.; Lee, K. M.; Jeong, J. R.; Friend, R. H.; Kim, J. S.; Kim, S. O.; Song, M. H. Highly Efficient Inverted Polymer Light-Emitting Diodes Using Surface Modifications of ZnO Layer. *Nat. Commun.* **2014**, *5*, 4840.

(10) Bolink, H. J.; Coronado, E.; Repetto, D.; Sessolo, M. Air Stable Hybrid Organic-Inorganic Light Emitting Diodes Using ZnO as the Cathode. *Appl. Phys. Lett.* **2007**, *91*, 223501.

(11) Kabra, D.; Lu, L. P.; Song, M. H.; Snaith, H. J.; Friend, R. H. Efficient Single-Layer Polymer Light-Emitting Diodes. *Adv. Mater.* **2010**, *22*, 3194−3189.

(12) Hofle, S.; Schienle, A.; Bruns, M.; Lemmer, U.; Colsmann, A. Enhanced Electron Injection into Inverted Polymer Light-Emitting

DOI: 10.1021/acsami.5b05815
ACS Appl. Mater. Interfaces 2015, 7, 20769−20778

Diodes by Combined Solution-Processed Zinc Oxide/Polyethylenimine Interlayers. *Adv. Mater.* **2014**, *26*, 2750−2754.
(13) Bolink, H. J.; Coronado, E.; Orozco, J.; Sessolo, M. Efficient Polymer Light-Emitting Diode Using Air-Stable Metal Oxides as Electrodes. *Adv. Mater.* **2009**, *21*, 79−82.
(14) Lu, L. P.; Kabra, D.; Johnson, K.; Friend, R. H. Charge-Carrier Balance and Color Purity in Polyfluorene Polymer Blends for Blue Light-Emitting Diodes. *Adv. Funct. Mater.* **2012**, *22*, 144−150.
(15) Bolink, H. J.; Brine, H.; Coronado, E.; Sessolo, M. Ionically Assisted Charge Injection in Hybrid Organic-Inorganic Light-Emitting Diodes. *ACS Appl. Mater. Interfaces* **2010**, *2*, 2694−2698.
(16) Bolink, H. J.; Coronado, E.; Sessolo, M. White Hybrid Organic-Inorganic Light-Emitting Diode Using ZnO as the Air-Stable Cathode. *Chem. Mater.* **2009**, *21*, 439−441.
(17) Yook, K. S.; Lee, J. Y. Small-molecule Host Materials for Solution Processed Phosphorescent Organic Light-Emitting Diodes. *Adv. Mater.* **2014**, *26*, 4218−4234.
(18) Liao, H. H.; Chen, L. M.; Xu, Z.; Li, G.; Yang, Y. Highly Efficient Inverted Polymer Solar Cell by Low Temperature Annealing of Cs_2CO_3 Interlayer. *Appl. Phys. Lett.* **2008**, *92*, 173303.
(19) Li, G.; Chu, C. W.; Shrotriya, V.; Huang, J.; Yang, Y. Efficient inverted polymer solar cells. *Appl. Phys. Lett.* **2006**, *88*, 253503.
(20) Bolink, H. J.; Brine, H.; Coronado, E.; Sessolo, M. Phosphorescent Hybrid Organic-Inorganic Light-Emitting Diodes. *Adv. Mater.* **2010**, *22*, 2198−2201.
(21) Duan, C.; Zhang, K.; Zhong, C.; Huang, F.; Cao, Y. Recent Advances in Water/Alcohol-Soluble Pi-Conjugated Materials: New Materials and Growing Applications in Solar Cells. *Chem. Soc. Rev.* **2013**, *42*, 9071−9104.
(22) Huang, F.; Wu, H.; Cao, Y. Water/Alcohol Soluble Conjugated Polymers as Highly Efficient Electron Transporting/Injection Layer in Optoelectronic Devices. *Chem. Soc. Rev.* **2010**, *39*, 2500−2521.
(23) Zhou, Y.; Fuentes-Hernandez, C.; Shim, J.; Meyer, J.; Giordano, A. J.; Li, H.; Winget, P.; Papadopoulos, T.; Cheun, H.; Kim, J.; Fenoll, M.; Dindar, A.; Haske, W.; Najafabadi, E.; Khan, T. M.; Sojoudi, H.; Barlow, S.; Graham, S.; Brédas, J. L.; Marder, S. R.; Kahn, A.; Kippelen, B. A Universal Method to Produce Low-Work Function Electrodes for Organic Electronics. *Science* **2012**, *336*, 327−332.
(24) Xiong, T.; Wang, F.; Qiao, X.; Ma, D. A Soluble Nonionic Surfactant as Electron Injection Material for High-Efficiency Inverted Bottom-Emission Organic Light Emitting Diodes. *Appl. Phys. Lett.* **2008**, *93*, 123310.
(25) Wang, R.; Fan, C.; Xiong, Z.; Yang, X.; Jabbour, G. E. High-Efficiency Hybrid Organic-Inorganic Light-Emitting Devices. *Org. Electron.* **2015**, *19*, 105−112.
(26) Baek, H. I.; Lee, C.; Chin, B. D. Comparison of the Carrier Mobility, Unipolar Conduction, and Light Emitting Characteristics of Phosphorescent Host-Dopant System. *Synth. Met.* **2012**, *162*, 2355−2360.
(27) Zhang, Z.; Yan, P.; Yue, S.; Xie, G.; Chen, Y.; Wu, Q.; Qu, D.; Zhao, Y.; Liu, S. High Performance Top-Emitting and Transparent White Organic Light-Emitting Diodes Based on Al/Cu/TcTa Transparent Electrodes for Active Matrix Displays and Lighting Applications. *Org. Electron.* **2013**, *14*, 1452−1457.
(28) Yeh, H. C.; Meng, H. F.; Lin, H. W.; Chao, T. C.; Tseng, M. R.; Zan, H. W. All-Small-Molecule Efficient White Organic Light-Emitting Diodes by Multi-Layer Blade Coating. *Org. Electron.* **2012**, *13*, 914−918.
(29) Sun, Y.; Seo, J. H.; Takacs, C. J.; Seifter, J.; Heeger, A. J. Inverted Polymer Solar Cells Integrated with a Low-Temperature-Annealed Sol-Gel-Derived ZnO Film as an Electron Transport Layer. *Adv. Mater.* **2011**, *23*, 1679−1683.
(30) Tsang, D. P. K.; Chan, M. Y.; Tam, A. Y. Y.; Yam, V. W. W. Host Engineering for Improving the Performance of Blue Phosphorescent Organic Light-Emitting Devices. *Org. Electron.* **2011**, *12*, 1114−1119.
(31) Chang, Y. T.; Chang, J. K.; Lee, Y. T.; Wang, P. S.; Wu, J. L.; Hsu, C. C.; Wu, I. W.; Tseng, W. H.; Pi, T. W.; Chen, C. T.; Wu, C. I. High-Efficiency Small-Molecule-Based Organic Light Emitting Devices with Solution Processes and Oxadiazole-Based Electron Transport Materials. *ACS Appl. Mater. Interfaces* **2013**, *5*, 10614−10622.
(32) Yang, X.; Wang, R.; Fan, C.; Li, G.; Xiong, Z.; Jabbour, G. E. Ethoxylated Polyethylenimine as an Efficient Electron Injection Layer for Conventional and Inverted Polymer Light Emitting Diodes. *Org. Electron.* **2014**, *15*, 2387−2394.
(33) Lee, T. W.; Noh, T.; Shin, H. W.; Kwon, O.; Park, J. J.; Choi, B. K.; Kim, M. S.; Shin, D. W.; Kim, Y. R. Characteristics of Solution-Processed Small-Molecule Organic Films and Light-Emitting Diodes Compared with their Vacuum-Deposited Counterparts. *Adv. Funct. Mater.* **2009**, *19*, 1625−1630.
(34) Park, J.; Park, T.; Jeon, W.; Pode, R.; Jang, J.; Kwon, J.; Yu, E.; Chae, M. Small-molecule Interlayer for Solution Processed Phosphorescent Organic Light Emitting Device. *Org. Electron.* **2009**, *10*, 189−193.
(35) Nardes, A. M.; Kemerink, M.; De Kok, M. M.; Vinken, E.; Maturova, K.; Janssen, R. A. J. Conductivity, Work Function, and Environment al Stability of PEDOT:PSS Thin Films Treated with Sorbitol. *Org. Electron.* **2008**, *9*, 727−734.
(36) Guo, Y.; Robertson, J. Origin of the high work function and high conductivity of MoO_3. *Appl. Phys. Lett.* **2014**, *105*, 222110.
(37) Kim, H.; Byun, Y.; Das, R. R.; Choi, B. K.; Ahn, P. S. Small-molecule Based and Solution Processed Highly Efficient Red Electrophosphorescent Organic Light Emitting Devices. *Appl. Phys. Lett.* **2007**, *91*, 093512.
(38) Feng, S.; Duan, L.; Hou, L.; Qiao, J.; Zhang, D.; Dong, G.; Wang, L.; Qiu, Y. A Comparison Study of the Organic Small Molecular Thin Films Prepared by Solution Process and Vacuum Deposition: Roughness, Hydrophilicity, Absorption, Photoluminescence, Density, Mobility, and Electroluminescence. *J. Phys. Chem. C* **2011**, *115*, 14278−14284.
(39) Lv, Y.; Zhou, P.; Wei, N.; Peng, K.; Yu, J.; Wei, B.; Wang, Z.; Li, C. Improved Hole-Transporting Properties of Ir Complex-Doped Organic Layer for High-Efficiency Organic Light-Emitting Diodes. *Org. Electron.* **2013**, *14*, 124−130.
(40) Huang, F.; Shih, P. I.; Shu, C. F.; Chi, Y.; Jen, A. K. Y. Highly Efficient Polymer White-Light-Emitting Diodes Based on Lithium Salts Doped Electron Transporting Layer. *Adv. Mater.* **2009**, *21*, 361−365.
(41) Hou, L.; Duan, L.; Qiao, J.; Zhang, D.; Dong, G.; Wang, L.; Qiu, Y. Efficient Solution-Processed Small-Molecule Single Emitting Layer Electrophosphorescent White Light-Emitting Diodes. *Org. Electron.* **2010**, *11*, 1344−1350.
(42) Lee, J.; Lee, J. I.; Song, K. I.; Lee, S. J.; Chu, H. Y. Influence of Doping Profile on the Efficiency of Blue Phosphorescent Organic Light Emitting Diodes. *Appl. Phys. Lett.* **2008**, *92*, 133304.
(43) Baldo, M. A.; Adachi, C.; Forrest, C. S. R. Transient Analysis of Organic Electrophosphorescence. II. Transient Analysis of Triplet-Triplet Annihilation. *Phys. Rev. B: Condens. Matter Mater. Phys.* **2000**, *62*, 10967−10977.
(44) Reineke, S.; Walzer, K.; Leo, K. Triplet-Exciton Quenching in Organic Phosphorescent Light-Emitting Diodes with Ir-Based Emitters. *Phys. Rev. B: Condens. Matter Mater. Phys.* **2007**, *75*, 125328−125341.
(45) Chen, Y.; Chen, J.; Zhao, Y.; Ma, D. High Efficiency Blue Phosphorescent Organic Light-Emitting Diode Based on Blend of Hole- and Electron-Transporting Materials as a Co-Host. *Appl. Phys. Lett.* **2012**, *100*, 213301.
(46) Jou, J. H.; Peng, S. H.; Chiang, C. I.; Chen, Y. L.; Lin, Y. X.; Jou, Y. C.; Chen, C. H.; Li, C. J.; Wang, W. B.; Shen, S. M.; Chen, S. Z.; Wei, M. K.; Sun, Y. S.; Hung, H. W.; Liu, M. C.; Lin, Y. P.; Li, J. Y.; Wang, C. W. High Efficiency Yellow Organic Light-Emitting Diodes with a Solution-Processed Molecular Host-Based Emissive Layer. *J. Mater. Chem. C* **2013**, *1*, 1680−1686.
(47) Dumur, F.; Lepeltier, M.; Zamani Siboni, H.; Xiao, P.; Graff, B.; Lalevée, J.; Gigmes, D.; Aziz, H. Concentration-Insensitive Phosphorescent Organic Light Emitting Devices(PhOLEDs) for Easy Manufacturing. *J. Lumin.* **2014**, *151*, 34−40.

DOI: 10.1021/acsami.5b05815
ACS Appl. Mater. Interfaces 2015, 7, 20769−20778

(48) Li, G.; Feng, Y.; Peng, T.; Ye, K.; Liu, Y.; Wang, Y. Highly Efficient, Little Efficiency Roll-Off Orange-Red Electrophosphorescent Devices Based on a Bipolar Iridium Complex. *J. Mater. Chem. C* **2015**, *3*, 1452−1456.
(49) Lee, B. R.; Lee, S.; P ark, J. H.; Jung, E. D.; Yu, J. C.; Nam, Y. S.; Heo, J.; Kim, J. Y.; Kim, B. S.; Song, M. H. Amine-Based Interfacial Molecules for Inverted Polymer-Based Optoelectronic Devices. *Adv. Mater.* **2015**, *27*, 3553−3559.

DOI: 10.1021/acsami.5b05815
ACS Appl. Mater. Interfaces 2015, 7, 20769−20778